AD_____
(Leave blank)

Award Number:
W81XWH-07-1-0454

TITLE:

Photonic Breast Tomography and Tumor Aggressiveness Assessment

PRINCIPAL INVESTIGATOR:

S. K. Gayen, Ph. D.

CONTRACTING ORGANIZATION:
University of New York City
New York, NY 10019-2925

REPORT DATE:
July 2010

TYPE OF REPORT:

Annual Summary

PREPARED FOR: U.S. Army Medical Research and Materiel Command
               Fort Detrick, Maryland 21702-5012

DISTRIBUTION STATEMENT: (Check one)

    X Approved for public release; distribution unlimited

    ☐ Distribution limited to U.S. Government agencies only;
       report contains proprietary information

REPORT DOCUMENTATION PAGE

Form Approved
OMB No. 0704-0188

1. REPORT DATE (DD-MM-YYYY) 14-Jul-2010	2. REPORT TYPE Annual Summary	3. DATES COVERED (From - To) 15 JUN 2009 – 14 JUN 2010
4. TITLE AND SUBTITLE Photonic Breast Tomography and Tumor Aggressiveness Assessment		**5a. CONTRACT NUMBER** W81XWH-07-1-0454
		5b. GRANT NUMBER W81XWH-07-1-0454
		5c. PROGRAM ELEMENT NUMBER
6. AUTHOR(S) S. K. Gayen Email: gayen@sci.ccny.cuny.edu		**5d. PROJECT NUMBER**
		5e. TASK NUMBER
		5f. WORK UNIT NUMBER
7. PERFORMING ORGANIZATION NAME(S) AND ADDRESS(ES) University of New York City Regina Masterson 555 West 57th Street, 11th Fl. New York, NY 10019-2925		**8. PERFORMING ORGANIZATION REPORT NUMBER**
9. SPONSORING / MONITORING AGENCY NAME(S) AND ADDRESS(ES) US Army Med. Res. Acq. Activity Attn.: MCMR-AAA-R (Monica Pileggi) 820 Chandler Street Fort Detrick, MD 21702-5014 Email:monica.pileggi@det.amedd.army.mil		**10. SPONSOR/MONITOR'S ACRONYM(S)** USAMRAA
		11. SPONSOR/MONITOR'S REPORT NUMBER(S)

12. DISTRIBUTION / AVAILABILITY STATEMENT

Approved for public release; Distribution unlimited

13. SUPPLEMENTARY NOTES

14. ABSTRACT

The tasks performed and the progresses made during the third year include: (a) participation in magnetic resonance (MR) imaging and spectroscopy experiments for lactate detection following training at the Memorial Sloan Kettering Cancer Center (MSKCC); and (b) conducting research on development of non-invasive optical imaging and spectroscopic approaches for breast tumor detection. The CCNY researchers constructed specialized coils for sensitive MR investigation, developed lactate phantoms, and investigated the feasibility of lactate concentration measurement at the MSKCC MR facility. Accurate *in vivo* measurement of lactate concentration in an animal model is expected to help assess if a tumor is fast growing, or slow growing. The near-infrared optical imaging research involved development of time reversal optical tomography (TROT) approach for imaging of absorbing target(s), OPTICA (optical tomography using independent component analysis) investigation for locating tumors in a realistic model cancerous breast assembled using *ex vivo* breast tissues. OPTICA could locate both the tumors, and the results agreed well with the results of MRI investigation of the same model breast. A new research proposal was developed and submitted to CDMRP 2010 BCRP Idea Award category for funding.

15. SUBJECT TERMS
Breast cancer, near-infrared imaging, optical tomography, independent component analysis, time reversal optical tomography, finite element method, image reconstruction, lactate detection, magnetic resonance spectroscopy and imaging

16. SECURITY CLASSIFICATION OF:			17. LIMITATION OF ABSTRACT	18. NUMBER OF PAGES	19a. NAME OF RESPONSIBLE PERSON S. K. Gayen
a. REPORT Unclassified	**b. ABSTRACT** Unclassified	**c. THIS PAGE** Unclassified	Unclassified	43	**19b. TELEPHONE NUMBER** (include area code) (212) 650-5580

Table of Contents

Page

4. INTRODUCTION

The HBCU/MI Partnership Training Award project, "*Photonic Breast Tomography and Tumor Aggressiveness Assessment*," is designed to establish a breast cancer training and research program at the City College of New York (CCNY) through close collaboration with the researchers at the Memorial Sloan Kettering Cancer Center (MSKCC). The focus of the training component of the project is to familiarize the CCNY researchers who happen to be physical scientists and engineers to the biological aspects of cancer research through attending relevant courses, and cancer research practicum through laboratory rotations. The objectives of the research component of the project are to develop optical imaging and spectroscopic approaches to (a) distinguish between aggressive and slow growing, metastatic and non-metastatic tumors, (b) non-invasively detect and diagnose breast tumors at early stages of growth.

During the *third* reporting period (June 15, 2009 – June 14, 2010) covered by this report, the training received during the first two years has been put into practice to initiate research on magnetic resonance imaging (MRI) approaches for distinguishing between aggressive and slow growing tumors. Concurrently, the research on developing near-infrared (NIR) light-based experimental methods and numerical algorithms for tumor detection has been pursued.

5. BODY

The tasks performed and the progresses made during the current reporting period are as follows:

- Translation of training to research on developing MRI approaches for studying tumor aggressiveness at MSKCC; and

- Pursuing research on development of non-invasive optical imaging and spectroscopic approaches for breast tumor detection.

We provide a brief outline of activities and accomplishments in these areas, and refer to appended materials for detailed description where applicable.

5.1. Translation of Training to Research: MRI Detection of Lactate

The training received by CCNY researchers (*Specific Aim 0, Task 2, Task 3 and Task 5*) at MSKCC prepared them for carrying out research on tumor aggressiveness assessment using the magnetic resonance imaging and spectroscopy (MRIS) facilities in primary collaborating mentor (PCM) Dr. Koutcher's lab at MSKCC. The focus was on developing MRIS approaches for detection of lactate, which is expected to provide a window to explore tumor aggressiveness (*Specific Aim 1*).

The interest in lactate detection stems from the fact that lactate level is associated with tumor aggressiveness, metastasis and treatment response [1,2]. As an end product of glycolysis metabolic pathway, lactate is considered as a prognostic marker of poor outcome in many tumors. Tumor lactate accumulation is caused by both aerobic glycolysis, a hallmark of tumors, and by anaerobic glycolysis in the hypoxia region of tumors. The development of non-invasive lactate detection methods is highly desirable for clinical evaluation. MRIS has been recognized as a promising technique for lactate detection. However, the overlapping lipid and adjacent water signals obscure lactate in the conventional MRSI. Over the last few years, the double frequency-selective multiple quantum coherence transfer (SelMQC) technique was developed to detect lactate [3].

4

In the third year of the project, the trainees validated the SelMQC technique for tumor aggressive assessment by phantom study. The major tasks that were under taken include:

- Implementation and optimization of the SelMQC on Bruker 4.7T spectrometer, and transfer the sequence to Bruker 7T spectrometer with higher field strength;
- Construct necessary radiofrequency (RF) coils and optimize the parameters for the phantom, next step for animal study;
- Fabricate phantoms and carry measurements on the phantoms.

The Signal-to-noise ratio (SNR) of the acquired lactate signal is sensitive to the field homogeneity. To achieve better homogeneity, several solenoid coils are necessary for tumors of different sizes. Coil with large diameter has lower resonance frequencies and worse homogeneity. As shown in Fig.1, two capacitors are used at both ends of the inductor instead of one series capacitor. In this way, both ends of the inductor experience the same voltage oscillation with π phase shift. The field homogeneity in the solenoid inductor is improved by this kind of symmetrical driving. To resolve the lower resonance frequencies issue in large coil, a capacitor is inserted into the inductor to center the RF coil's resonance frequency to 300 MHz as required by the Bruker 7T spectrometer. With the above improvements, achieve a high Q factor or quality factor of 200 for the big coil with 1.6 cm diameter was achieved. The 1.6 cm diameter coil can accommodate a tumor at the size of 1000 mm^3 for *in vivo* study.
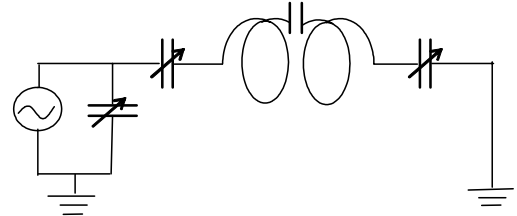

Fig. 1. Balanced solenoid coil for 7T

The next task was to fabricate lactate/water/lipid phantoms to optimize the coils and validate the SelMQC sequence for next step animal study. Lactate signals from phantoms with different lactate concentration and diameter sizes have been acquired. Figure 2 shows the chemical shift imaging (CSI) of the central 5 mm slice of a 10 mM lactate phantom by incorporating two-dimensional spatial encoding into SelMQC sequence. The peak in SelMQC-CSI shows the lactate signal in a voxel of 11.25 mm^3 with 1.5 mm in-plane resolution. The SelMQC-CSI is co-registered with T2-weighted image. The T1 and T2 relaxations of lactate in the phantom were measured to quantitatively determine the lactate concentration, which will be an important step in the *in vivo* study.

CSI 1986 11.25mm3, FOV=24, steps16, 10mM phantom NEX=4
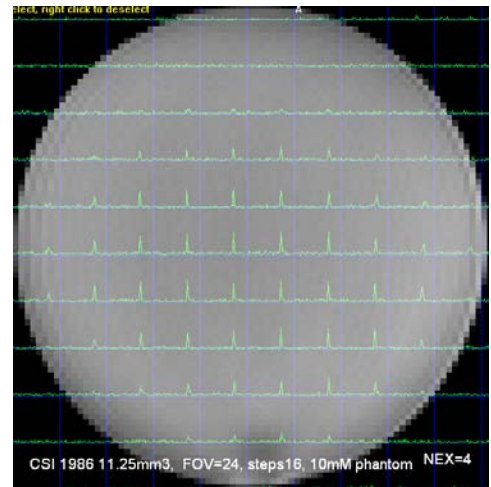
Fig. 2. SelMQC-CSI of 10 mM lactate phantom (co-registered with T2 image).

Tumor lactate level is in the 0-15 mM range according *in vitro* study. The results of the preliminary phantom study show the feasibility of *in vivo* lactate detection with the coils developed to date. They *in vivo* lactate study for aggressive and non-aggressive tumor models will be carried out and correlated with optical imaging technique developed at CCNY. We are developing the required IACUC protocol for agency approval.

5.2. Development of Near-Infrared Optical Imaging Modality for Breast Cancer Detection

We have pursued the work on development of non-invasive near-infrared optical imaging modalities for early detection of breast cancer (*Specific Aim 4*) that started during Year 1 of the project [4]. This research builds on and extends the work that the CCNY group has been pursuing.

The goal of the research is to develop optical spectroscopy and imaging approaches that use the near-infrared (800-1300 nm) light to obtain three-dimensional (3-*D*) tomographic images of human breast to enable detection, localization, and possible diagnosis of tumor(s) in the breast. Early detection of breast tumor with requisite sensitivity and specificity is a daunting task and we are pursuing different approaches, which are at different stages of development. During this reporting period we further extended the scope and tested the efficacy of the *optical tomographic imaging using independent component analysis* (OPTICA) [5,6] that we developed earlier, continued developing the new approach of *time reversal optical tomography* (TROT) [7-9], and initiated an adaptation of the *finite element method* (FEM) [10-12] for our experimental arrangements.

5.2.1. Multi-wavelength OPTICA studies a 'model cancerous breast'

We pursued further extension of OPTICA to include multi-wavelength probing and explored its efficacy on a more realistic model breast (*Specific Aim 4, Task #15 and Task #16*) that we reported in the Second Annual Report [13] for this project. The experimental arrangement for OPTICA, which we assembled (*Specific Aim 4, Task #14*) during the first reporting period [4], uses multi-source illumination of sample under investigation, and multi-detector transillumination signal acquisition. Light beams of wavelengths 750 nm, 800 nm, and 850 nm from a Ti-sapphire laser were used for probing the 'model cancerous breast' assembled using of *ex vivo* adipose tissues ((*Specific Aim 4, Task #15*) with two tumors (invasive ductal carcinoma) embedded within. The model breast was approximately a 100-mm diameter and 42-mm thick cylinder held together in a transparent plastic container. A 16-bit 1024 x 1024 pixels CCD camera record the transmitted signal. The sample was scanned across the laser beam in a 16x26 *x-y* array of grid points and a two-dimensional transmission image was recorded for each position for each wavelength to meet the multi-source multi-detector (each pixel of a CCD camera being a detector element) imaging arrangement required for OPTICA. The data acquisition time is less than 8 minutes for a 16x26 scan at one given wavelength. The resulting data was analyzed using the numerical algorithm of OPTICA [5,6]. The details of the experimental arrangement, data acquisition, processing and analysis methods are similar to that presented in the Annual Reports [4, 14] and a published paper [6].

The approach provided the locations of both the tumors in three dimensions with high accuracy. Multi-wavelength measurements enabled better discrimination of tumors from other components. A back-projection algorithm enabled estimation of the cross section of the tumors. The sample was further investigated using MRI and the results are in good agreement with the OPTICA estimates.

While a substantial part of this work was done during the second reporting period and was reported as such, during the current reporting period we presented the paper entitled, "*Multi-wavelength optical tomography using independent component analysis*," based on these results at

the NIH Inter-Institute Workshop on Optical Diagnostic and Biophotonic Methods from Bench to Bedside, (1-2 October 2009, Bethesda, Maryland) [14]. A copy of the abstract that appeared in the program bulletin fir Workshop is presented in *Appendix 1*.

A manuscript based on these results has been prepared and being finalized for submission in a professional journal (*Appendix 2*).

5.2.2. Development of Time Reversal Optical Tomography

We have pursued development of the *Time Reversal Optical Tomography* (TROT) approach, which we first reported in the Second Annual Report [13.], in our ongoing quest for fast and accurate methods for detection and localization of tumours in breast, and for detection of margins during surgical removal of breast tumours (*Specific Aim 4*). While the TROT approach [7] has been introduced in other areas, such as, array processing for acoustic and radar time-reversal imaging, we are beginning to implement it [8,9] for optical tomographic imaging of breast. Some of the initial work was presented in a conference [9], and the abstract of that conference is presented as *Appendix 3*.

TROT is based on multi-static data and vector subspace classification to eigenvectors of a round-trip matrix. In optical imaging application, a *response matrix* represents the transport of light from multiple sources through a turbid medium with embedded targets to an array of detectors. The response matrix is constructed from the experimental data that represent the perturbation on the sample boundary due to the presence of target(s). The 'round-trip (RT) matrix' is constructed by multiplying the response matrix by its transpose matrix for continuous wave illumination (by adjoint matrix for frequency-domain case). Mathematically, the RT matrix is equivalent to transfer of light from multiple sources through a turbid medium with embedded targets to an array of detectors, and back, and is similar to the time-reversal matrix used in the general area of array processing for acoustic and radar time-reversal imaging [15]. The eigenvalue equation of TR matrix is solved, and the signal and noise are separated into orthogonal subspaces, using an L-curve regularization method. Then a pseudo spectrum [Eq.(1) in Ref. 8] is calculated directly for all voxels in the sample using the vector subspace method, Multiple Signal Classification (MUSIC) [7,8]. Pseudo tomographic images can be generated using pseudo values. Locations of targets are determined by the global maxima (or local maxima in low SNR case) components in the pseudo spectrum. Compared to other inverse methods, which usually require iterations, TROT is fast since there is no iteration involved.

We have investigated the efficacy of TROT by imaging absorptive target(s) embedded in Intralipid-20% suspension in water, a model medium whose optical absorption and scattering properties can be adjusted by varying the concentration. We attempted to address two important issues: (i) how the accuracy of retrieved target position depends on the absorption contrast, and target location; and (ii) how close two targets can be and still the images be resolved.

The sample was a 250 mm $\times$ 250 mm $\times$ 60 mm transparent plastic container filled with Intralipid-20% suspension in water. The concentration of Intralipid-20% was adjusted to provide an absorption coefficient $\mu_a \sim 0.003$ mm^{-1} and a transport mean free path, $l_t \sim 1$ mm at 790 nm, which emulate the average values of those parameters for human breast tissue. Two different experiments were carried out with absorptive targets. In Experiment 1, the depth (distance from the input or source plane along the axial, *z*-direction) of a single target was varied keeping the lateral (*x-y*) positions same to explore how the spatial resolution changed with depth. In Experiment 2, the separation between two targets along *x*-axis was varied keeping the (*y, z*) positions fixed to

investigate spatial resolution along a lateral direction. The target(s) were glass sphere(s) of diameter ~9 mm filled with ink (absorber) dissolved in Intralipid-20% suspension in water. The absorption coefficient of the targets was μ_a =0.013 mm^{-1} which was about 3 times higher than that of background medium, while the scattering coefficient μ_s was adjusted to be the same as that of the background medium. The target locations used in the experiments are presented in Table I and Table II, respectively. The sample was scanned with a 790-nm diode-laser beam in an array of 9×9 grid points for Experiment 1 and 11×15 grid points for Experiment 2 with a step size of 5 mm. A 1024×1024 pixels CCD camera recorded the transmitted signal as 2-D images of the exit (detection) plane, which was the raw data to be used in the subsequent analysis.

The key results from Experiment 1 that maintains the same lateral position (*x, y*) for both the targets but varies the axial position (*z* = 15 mm, 20 mm, 25 mm, 30 mm, 35 mm, 40 mm, and 45 mm) are:

- Both the *lateral positions* (*x, y*) and the *axial positions* (*z, depth*) of the target are retrieved with substantial accuracy.

- The *lateral positions* are determined with better accuracy (error range of 0.2 mm - 1 mm compared to known values) than the *axial position* (error range of 0.5 mm – 3 mm). The errors are dependent on the axial position (depth) of the target.

- The errors are higher when the target is closer to the sample boundaries than when it is closer to the center, which may be attributed to 'boundary effect' that will be further investigated.

- While the target position is determined with identical high accuracy when the target is near the center of the sample, away from the center the error is smaller for target with higher contrast (μ_a =1.0 mm^{-1}) than that with lower contrast (μ_a =0.013 mm^{-1}).

Experiment 2 revealed that both the targets could be resolved even when their nearby surfaces were separated by a distance of ~ 4 mm (center-to-center distance of ~ 13 mm). Fig. 3 shows a typical reconstructed image of the two targets. The resolution was found to be higher when the targets were further apart than when those were closer together.
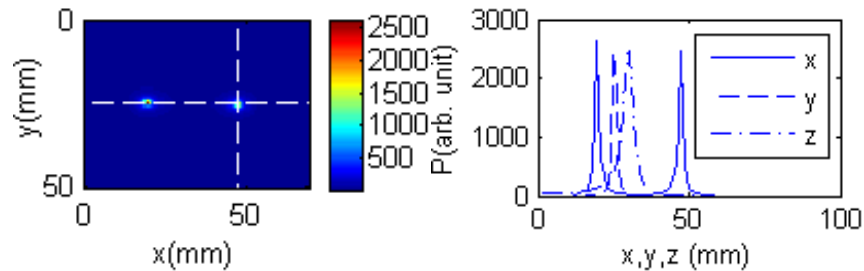

Fig 3. TROT generated cross-section pseudo image of the right target when they were separated by 27.6 mm in Exp. 2 is shown in the left pane and pseudo-value profiles through the target along x, y and z directions shown in the right pane.

The results obtained so far for absorbing targets make TROT a promising approach for optical mammography. A paper entitled, *"Three-dimensional time-reversal optical tomography"* has been submitted for the SPIE's 2011 BiOS Conference. Future plan includes pursuing detection and localization of scattering targets, targets that are both scattering and absorbing, to be followed by realistic model breast assembled using *ex vivo* beast tissues.

5.2.3. Finite Element Method for Optical Tomography

We are exploring the Finite Element Method (FEM) that has found considerable use in optical tomography [10-12], as another viable approach to optical mammography (*Specific Aim 4, Task# 17 and Task# 18*). FEM attempts to derive photon density inside a sample and photon flux at its boundary by using the diffusion model to describe light propagation in highly scattering media. In FEM, the object domain Ω is partitioned into finite number of elements which join at D vertex nodes to construct the so-called mesh. Using the Galerkin method, the nodal solutions are found, and the solution everywhere in the domain is approximately piecewise linearly interpolated using the nodal solutions. In the image obtained by FEM, the resolution is limited by the width of the photon measurement density function, *i.e.,* the area over which a measurement for a given source–detector pair is sensitive to a change in the optical properties [10,11]. Compared to Monte Carlo method, reconstruction based on FEM is faster.

A forward model is built to calculate the measurements on the detectors using the known sources, detectors and properties of the object along with an appropriate model to describe light propagation. For image reconstruction, the sources, detectors and measurements on the detectors are given along with the light propagation model. The properties (μ_a and μ_s) of the object are retrieved by using a non-linear optimization method, such as, the Gauss-Newton method or gradient descent method that iteratively calls the forward model and seeks to minimize the error between the measurements on the object boundary calculated with the forward model and the experimental ones.

We are adapting a toolbox called Time-resolved Optical Absorption and Scattering Tomography (TOAST) developed by Schweiger and Arridge at the University College London [12]. TOAST can be used with data obtained using time-domain, frequency domain and continuous wave (CW) experimental methods. As a first step, we are using the simulated CW data. Different meshes, object optical properties, source and detector pairs etc were tried to optimize the model for different experimental conditions.
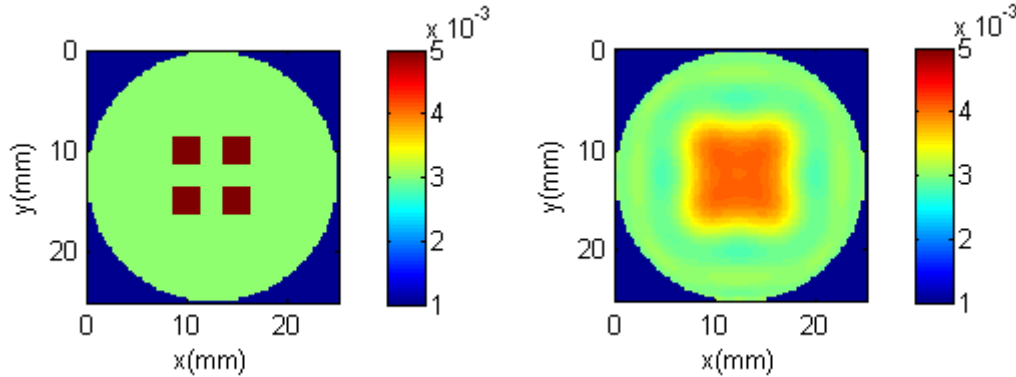

Fig. 4: Left pane: four targets in the circular sample; right pane: reconstructed targets

We have tested the approach with 2D conditions. Along the line of Reference 11 for simulating human skull for brain imaging, we consider a circular sample of radius 12.5 mm, with 4 targets of μ_a =0.06 mm^{-1} and same μ_s as that of background embedded in the center of the circle and separated by 5mm from the nearby ones, as shown in the left pane of Fig. 4. The optical properties of the background were taken to be μ_a = 0.003 mm^{-1}, l_t = 1 mm^{-1} which simulates the NIR properties of human breast tissue, and of the target to be μ_a = 0.006 mm^{-1}. 32 sources and 32 detectors are place around the edge of the circle. 10-node triangular elements are used to create the

mesh. The reconstructed image for a simulated breast phantom shown in the right pane does not resolve the targets as well as in Reference 11 that considers human brain.

We also tested a square sample as shown in Fig. 5 (left), of side 50 mm, $\mu_a = 0.003$ mm^{-1} and l_t = 1 mm. Four targets with μ_a =0.006 mm^{-1} and same μ_s as that of background were embedded in the central region of the sample and separated by 25 mm from the nearby ones. 9 sources and 9 detectors were placed along each size of the square. 4-node rectangular elements were used to create the mesh. An arbitrary Jacobian matrix that maps the sensitivity of measurement on the surface of an object to the perturbation of the optical parameters within the object is shown in Fig.5 (middle). The reconstructed targets are shown in Fig.5 (right). Even though we can see the four targets clearly in the reconstructed image, the contrast $(I_{max} - I_{min})/(I_{max} + I_{min})$ is actually very low. Different meshes, number and positions of sources and detectors all change the result a lot. We are pursuing this work to enhance resolution and contrast.
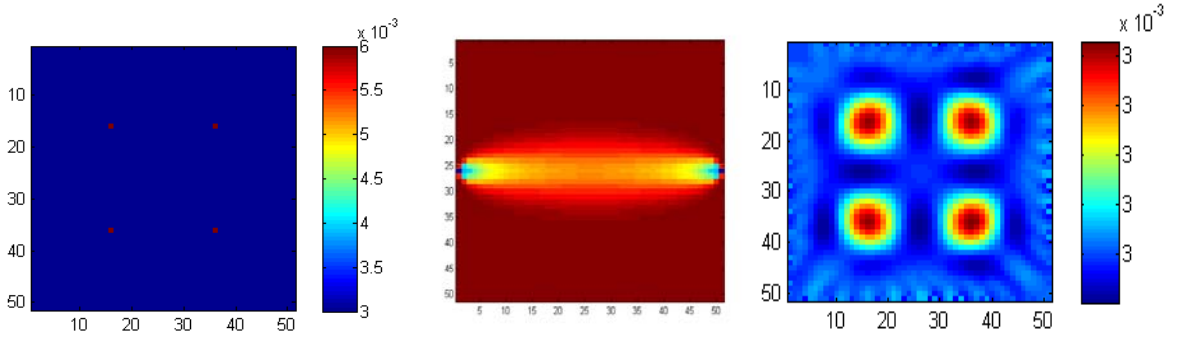

Fig. 5: Left pane: four targets in the circular sample; middle pane: Jacobian; right pane: reconstructed targets

For 3D case, we have started with a 250 mm × 250 mm × 40 mm, simulated sample of $\mu_a =$ 0.003 mm^{-1}, and $\mu_s = 1$ mm^{-1}. 8-node tetrahedron elements are used to create the mesh, as shown in Fig. 6. A forward projection of a point source located at $z = 1$mm and detected on $z = 40$ mm is shown in Fig.6 (right) without any target embedded in the sample.
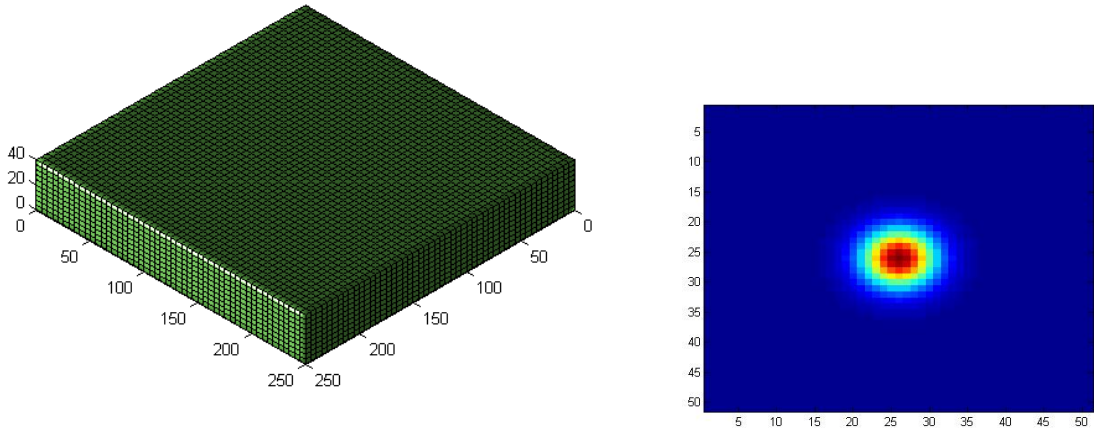

Fig. 6: Left pane: mesh; right pane: forward projection of a point source

10

To check the goodness of the forward model, we compared the forward projection to the analytical result and they fit very well. The linearity of the perturbation of a point target was also examined, which confirmed that for weak perturbation, the change in the optical measurement is linear with respect to the perturbation in the optical property of the inhomogeneity.

We plan to pursue the FEM approach further for 3D image reconstruction and estimation of target optical properties.

5.3. Research Proposal Development

One of the proposed tasks (*Specific Aim 0, Task# 7*) involves developing at least one research proposal and submitting it to NIH or USAMRMC for funding. Accordingly, we have developed a research proposal entitled, "*Nanocomposite-Chemokine Mimic Conjugates for Imaging and Prevention of Breast Cancer Metastases*" and submitted to the Idea Award (Collaborative Option) category of the 2010 Breast Cancer Research Program of CDMRP. S. K. Gayen (PI of this proposal) is the Initiating PI of the above-mentioned proposal. The Collaborative PI is Valeria Balogh-Nair of the CCNY Chemistry Department.

The *objectives* of the proposed research are to demonstrate that: (a) breast cancer metastases can be prevented by blocking cell migration using self-targeting nanoparticle-chemokine mimic conjugates that will encompass an imaging module and a therapeutic module within the same nanostructure; and (b) near-infrared imaging using the imaging module, as well as, the conjugate of imaging and therapeutic module as fluorescent contrast agents will provide high contrast images of tumors at early stages of growth and facilitate early detection. Diagnosis and treatment will be achieved with a single conjugate module. Moreover, using the chemokine mimics to make the conjugate self targeting and multivalency built into the therapeutic module allow to bypass the use of tumor-homing devices that suffer from clinical limitations (e.g., antibodies, peptides, viral vectors), and will afford high local concentrations of the therapeutic module that in turn will help to achieve high drug efficacy.

A copy of the technical abstract of the proposal is attached as *Appendix 4* to this report.

6. KEY ACCOMPLISHMENTS

- The key training accomplishment includes the successful participation of physical scientists and engineers of CCNY research team in cancer biology research involving magnetic resonance spectroscopic imaging at the MRI research facility of MSKCC.

- Key research accomplishments include: (a) demonstration of the efficacy of Optical Tomography using Independent Component Analysis (OPTICA) approach for detection, 3-*D* localization, and cross section imaging of two tumors inside a realistic breast model composed of excised breast tissues; (b) development of the Time Reversal Optical Tomography (TROT) approach as a potential optical mammography method; and (c) lactate detection using magnetic resonance spectroscopic imaging as a potential method for assessing tumor aggressiveness.

- Development and submission of an independent research proposal to BCRP 2010 is indicative of the CCNY team's progress towards developing a sustainable breast cancer research program at CCNY.

7. REPORTABLE OUTCOMES

Conference Presentations

(1) M. Alrubaiee, M. Xu, S. K, Gayen, V. Longo, and R. R. Alfano, *"Multi-wavelength optical tomography using independent component analysis*." Poster 53 presented at the NIH Inter-Institute Workshop on Optical Diagnostic and Biophotonic Methods from Bench to Bedside 2009, October 1-2, Bethesda, MD.

(2) Binlin Wu, M. Alrubaiee, W. Cai, M. Xu and S. K. Gayen, *"Optical imaging of objects in turbid media using Principal Component Analysis and Time Reversal Matrix Methods,"* in *Computational Optical Sensing and Imaging*, OSA Technical Digest (CD) (Optical Society of America, 2009), paper JTuC10. Presented at the Annual Meeting of the Optical Society of America, October 11-15, 2009, San Jose, California.

(3) Binlin Wu, M. Alrubaiee, W. Cai, M. Xu and S. K. Gayen, *"Three-dimensional time-reversal optical tomography,"* submitted to SPIE's 2011 BiOS Conference.

Manuscript

(1) M. Alrubaiee, M. Xu and S. K. Gayen, *"Multi-wavelength optical imaging using independent component analysis detects and locates tumors in an ex vivo model human breast"* to be submitted to *Applied Optics*.

Research Proposal

(1) S. K. Gayen (Initiating PI), V. Balogh-Nair (Collaborating PI), *"Nanocomposite-Chemokine Mimic Conjugates for Imaging and Prevention of Breast Cancer Metastases,"* submitted to the Idea Award (Collaborative Option) category of the 2010 Breast Cancer Research Program of CDMRP.

Student Progress

Binlin Wu, a graduate student supported by this grant passed his Second Examination during the current reporting period when he successfully defended his Ph. D. thesis proposal.

8. CONCLUSION

The work carried out during this reporting period: (a) culminated in CCNY research trainees' participation in magnetic resonance spectroscopic imaging breast cancer research at MSKCC; and (b) shows the potential for noninvasive detection and three-dimensional localization of a tumor within a breast with significant accuracy. The contrast is based on the differences in the light scattering and absorption characteristics of the tumor and normal breast tissue.

"So What Section"

- The National Cancer Institute (NCI) has identified the development of imaging methodologies as an extraordinary opportunity for advancement in cancer research. Since the background of the CCNY team is in physical sciences and engineering, the training they received has provided them with necessary laboratory background in the biology of cancer research, and helping develop a knowledgeable multidisciplinary research force in the fight against breast cancer.

- A recent study involving 35,319 patients underscores the influence of primary tumor location on breast cancer prognosis [16], and makes it imperative that breast cancer detection modalities to obtain three-dimensional (3-*D*) location of the tumor relative to the axilla be developed. The current work is an important development in obtaining 3-*D* location of a tumor within the breast.

- The study of model cancerous breast assembled using *ex vivo* breast tissues is important and essential for the next step, *in vivo* optical breast imaging involving volunteers.

- The study involving lactate detection holds promise for tumor aggressiveness assessment.

9. REFERENCES

1. A. Le, C. R. Cooper, A. M. Gouw, R. Dinavahi, A. Maitra, L. M. Deck, R. E. Royer, J. D. L. Vander, G. L. Semenza, C. V. Dang, "Inhibition of lactate dehydrogenase A induces oxidative stress and inhibits tumor progression," *Proc. Natl. Acad. Sci. USA* **107**, 2037 (2010).

2. Pierre Sonveaux, Frédérique Végran, Thies Schroeder, Melanie C. Wergin, Julien Verrax, Zahid N. Rabbani, Christophe J. De Saedeleer, Kelly M. Kennedy, Caroline Diepart, Bénédicte F. Jordan, Michael J. Kelley, Bernard Gallez, Miriam L. Wahl, Olivier Feron, Mark W. Dewhirst, "Targeting lactate-fueled respiration selectively kills hypoxic tumor cells in mice," *J. Clin. Invest.* **118**, 3930 (2008).

3. M. Muruganandham, J. A. Koutcher, G. Pizzorno, and Q. He, "*In vivo* tumor lactate relaxation measurements by selective multiple-quantum-coherence (Sel-MQC) transfer," *Magn. Reson. Med.* **52,** 902 (2004).

4. Annual Report Dated August 2008 covering the period 15 June 2007 – 14 June 2008, Award Number W81XWH-07-1-0454, on file at USAMRMC.

5. M. Alrubaiee, M. Xu, S. K. Gayen, M. Brito, and R. R. Alfano, "Three-dimensional optical tomographic imaging of objects in tissue-simulating turbid medium using independent component analysis," *Appl. Phys. Lett.* **87**, 191112 (2005).

6. M. Xu, M. Alrubaiee, S. K. Gayen and R. R. Alfano, "Optical diffuse imaging of an *ex vivo* model cancerous human breast using independent component analysis," *IEEE J. Select. Topics Quantum Electron.* **14**, 43 (2008).

7. A. J. Devaney, "Time reversal imaging of obscured targets from multi-static data," *IEEE. Trans. Ant & Prop.* **53,** 1600-1610 (2005).

8. W. Cai, M. Alrubaiee, S. K. Gayen, M. Xu, R. R. Alfano, "Three-dimensional optical tomography of objects in turbid media using the round-trip matrix," *Proc. SPIE* **5693**, 4 (2005).

9. Binlin Wu, M. Alrubaiee, W. Cai, M. Xu and S. K. Gayen, "*Optical imaging of objects in turbid media using Principal Component Analysis and Time Reversal Matrix Methods,*" in *Computational Optical Sensing and Imaging*, OSA Technical Digest (CD) (Optical Society of America, 2009), paper JTuC10. Presented at the Annual Meeting of the Optical Society of America, October 11-15, 2009, San Jose, California.

10. S. R. Arridge and M. Schweiger, "Photon measurement density functions. Part 2: Finite element calculations", *Appl. Opt.* **34**, 8026 (1995).

11. M. Schweiger and S. R. Arridge, "Optical tomographic reconstruction in a complex head model using a priori region boundary information", *Phys. Med. Biol.* **44**, 2703 (1999).

12. http://web4.cs.ucl.ac.uk/research/vis/toast/

13. Annual Report Dated August 2009 covering the period 15 June 2008 – 14 June 2009, Award Number W81XWH-07-1-0454, on file at USAMRMC.

14. M. Alrubaiee, M. Xu, S. K, Gayen, V. Longo, and R. R. Alfano, "*Multi-wavelength optical tomography using independent component analysis*." Poster 53 presented at the NIH Inter-Institute Workshop on Optical Diagnostic and Biophotonic Methods from Bench to Bedside 2009, October 1-2, Bethesda, MD.

15. C. Prada, J. L. Thomas, and M. Fink, "The iterative time-reversal process: analysis of the convergence," *J. Acoust. Soc. Am.* **97**, 62 (1995).

16. N. Kroman, J. Wohlfahrt, H. T. Mouridsen, and M. Melbye, "Influence of tumor location on breast cancer prognosis," *Int. J. Cancer* **105**, 542 -545 (2003).
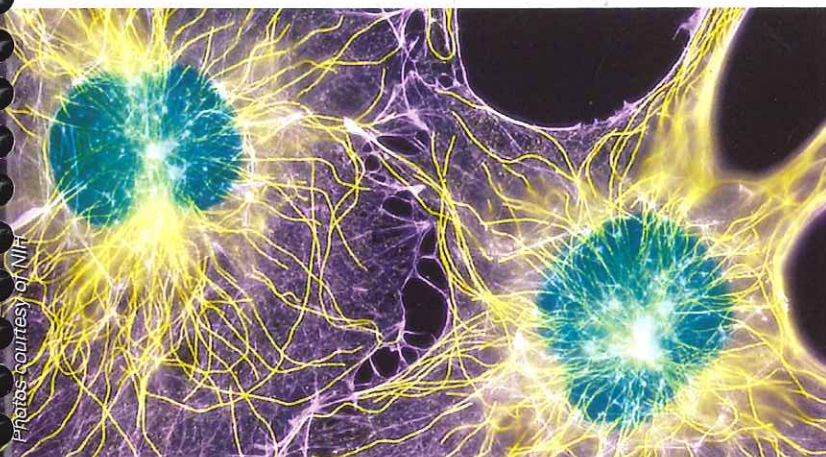
10. APPENDICES

Appendix 1. A copy of the abstract of: M. Alrubaiee, M. Xu, S. K, Gayen, V. Longo, and R. R. Alfano, "*Multi-wavelength optical tomography using independent component analysis*." Poster 53 presented at the NIH Inter-Institute Workshop on Optical Diagnostic and Biophotonic Methods from Bench to Bedside 2009, October 1-2, Bethesda, MD.

Appendix 2. A copy of a manuscript: M. Alrubaiee, M. Xu and S. K. Gayen, "*Multi-wavelength optical imaging using independent component analysis detects and locates tumors in an ex vivo model human breast*" to be submitted to *Applied Optics*.

Appendix 3. A copy of the abstract of a conference presentation: Binlin Wu, M. Alrubaiee, W. Cai, M. Xu and S. K. Gayen, "*Optical imaging of objects in turbid media using Principal Component Analysis and Time Reversal Matrix Methods,*" in *Computational Optical Sensing and Imaging*, OSA Technical Digest (CD) (Optical Society of America, 2009), paper JTuC10. Presented at the Annual Meeting of the Optical Society of America, October 11-15, 2009, San Jose, California.

Appendix 4. A copy of the technical abstract of a proposal: S. K. Gayen (Initiating PI), V. Balogh-Nair (Collaborating PI), "*Nanocomposite-Chemokine Mimic Conjugates for Imaging and Prevention of Breast Cancer Metastases,*" submitted to the Idea Award (Collaborative Option) category of the 2010 Breast Cancer Research Program of CDMRP.

Inter-Institute Workshop on Optical Diagnostic and Biophotonic Methods from Bench to Bedside

1–2 October 2009

Natcher Conference Center
National Institutes of Health
Bethesda, Maryland, USA

Organized by

SPIE
Connecting minds. Advancing light.

National Institutes of Health
The Nation's Medical Research Agency

Multi-wavelength optical tomography using independent component analysis

M. Alrubaiee, M. Xu, S. K. Gayen, The City College of New York (United States); V. A. Longo, Memorial Sloan-Kettering Cancer Ctr. (United States); R. R. Alfano, The City College of New York (United States)

Multi-wavelength optical imaging using independent component analysis (MW-OPTICA) of a realistic breast model composed of ex vivo human female breast tissue is presented. The sample was a 100 mm diameter and 42 mm thick cylinder formed predominantly of adipose tissues with two tumors (invasive ductal carcinoma) embedded within. The experimental arrangement used 750 nm, 800 nm, and 850 nm light from a Ti-sapphire laser to illuminate the sample, and a 16-bit 1024 x 1024 pixels CCD camera to record the signal. The sample was scanned across the laser beam in a 16x26 x-y array of grid points and a two-dimensional transmission image was recorded for each position for each wavelength to meet the multi-source multi-detector imaging arrangement required for OPTICA. The data acquisition time is less than 8 minutes for a 16x26 scan at one given wavelength. The resulting data was analyzed using the ICA formalism.

The approach provided the locations of both the tumors in three dimensions with high accuracy. Multi-wavelength measurements enabled better discrimination of tumors from other components. A back-projection algorithm enabled estimation of the cross section of the tumors. The sample was further investigated using x-ray computed tomography (CT) for comparison with and testing the efficacy of optical approach. MW-OPTICA results are in good agreement with CT results.

Multi-wavelength optical imaging using independent component analysis detects and locates tumors in an *ex vivo* model human breast

M. Alrubaiee

Institute for Ultrafast Spectroscopy and Lasers, Physics Department, City College and Graduate Center, City University of New York, New York, New York 10031, USA

M. Xu

 Department of Physics, Fairfield University, Fairfield, CT 06824, USA

S. K. Gayen

Physics Department, The City College and Graduate Center, City University of New York, New York, New York 10031, USA

_____

Address all correspondence to S. K. Gayen, The City College of the City University of New York, Department of Physics, 160 Convent Avenue, New York, NY 10031, USA, E-mail: gayen@sci.ccny.cuny.edu

Abstract

Optical imaging using independent component analysis (OPTICA) is used to detect, locate, and obtain cross-section images of two tumor pieces inside a model human breast assembled using *ex vivo* human breast tissues and configured as a semi-cylindrical slab of uniform thickness. The experimental arrangement realized a multisource probing scheme to illuminate an end face (source plane) of the slab sample using 750 nm, 800 nm and 830 nm beams of laser light. A multi-detector signal acquisition scheme measured transmitted light intensity distribution on the other end face (detection plane). This combined multisource probing and multi-detector sensing approach culminated in multiple spatial and angular views of the sample necessary for target localization. Independent component analysis of the perturbations in light intensity distribution in the detection plane sorted out signals originating from targets within the sample. Measurement using light of different wavelengths helped rule out a potential target as an artifact. A back-projection technique provided cross-section images and estimates of cross section of the targets within the sample. The estimated locations and dimensions of targets are in good agreement with the results of a corroborating magnetic resonance imaging experiment and known values.

Keywords: Breast cancer, near-infrared (NIR) imaging, inverse image reconstruction, medical imaging, magnetic resonance imaging, diffuse optical tomography, independent component analysis, absorption, scattering, diffusion, image processing

1. Introduction

Optical imaging using independent component analysis (OPTICA) is an emerging approach for detection and localization of targets embedded in a turbid medium, an important example being a tumor in human breast. The impetus for developing a noninvasive approach for detection of breast cancer with diagnostic potential led to the development of different diffuse imaging and inverse image reconstruction schemes using near-infrared (NIR) light.[1-9] However, reconstruction of images and determination of tumor location with high spatial resolution remains a challenging task. OPTICA is an alternative to above-mentioned diffuse optical tomography approaches with demonstrated ability to detect and locate small targets in model turbid media.[10-13]

OPTICA uses a multi-source probing and a multi-detector signal acquisition scheme to obtain multiple angular and spatial views of the turbid medium and generate a robust data set necessary for detection and localization of targets within the medium. Like other optical approaches, OPTICA treats the targets as inhomogeneities whose optical properties, such as, absorption coefficient and scattering coefficient differ from the average values of those properties for the surrounding medium. It further considers the targets independent, and the signal measured at the boundary of the medium to contain a weighted mixture of contributions from these independent targets. It then uses the independent component analysis (ICA),[14, 15] a statistical technique from information theory, to sort out independent components (ICs) that the independent targets contribute to the signal. Each IC serves as the staring point for obtaining the location of the corresponding target, since the IC relates to how the light propagates from the source to the target, and from the target to the detector. With this assessed target location, a back

projection of the corresponding IC onto the transversal plane at the axial location of the target

yields a two-dimensional cross section image of the target.

In this paper, we extend our previous studies[10-13] of OPTICA to a 'model' cancerous

human breast composed of *ex vivo* tissues with two tumor pieces embedded at two different

locations. There are suggestions in the literature, [3,7] that measurements using lights of different

wavelengths targeting different tissue constituents may provide clarifying information. We have

used lights of three different wavelengths and realized some advantages. We also investigated

the model breast using magnetic resonance imaging (MRI) to serve as a point of reference for

optical measurement. The rest of the paper is organized as follows. Section 2 presents a brief

overview of the theoretical formalism. Section 3 describes the experimental arrangement,

methods, materials, and parameters. Section 4 presents the experimental results, while Section 5

compares the optical results with that obtained from MRI and discusses their implications.

2. Theoretical Formalism

The theoretical formalism of optical imaging using independent component analysis with

multiple wavelengths is a natural extension of our earlier work on OPTICA with a single

wavelength. In this part, we will briefly review OPTICA for the case when data collected using

multiple wavelengths are used in analysis.

The presence of targets (optical inhomogeneities) inside a turbid medium perturbs the

spatial intensity distribution of light emergent from the medium under illumination by a probing

beam. When probed by a point light source of unit power, the change in the light intensity

distribution on the sample boundary due to embedded absorptive and scattering targets can be

written as[16, 17]

$$-\Delta I(\mathbf{r}_d, \mathbf{r}_s; \lambda) = \int d^3 r \delta\mu_a(\mathbf{r}, \lambda) c G(\mathbf{r}_d, \mathbf{r}; \lambda) G(\mathbf{r}, \mathbf{r}_s; \lambda)$$
$$+ \int d^3 r \delta D(\mathbf{r}, \lambda) c \nabla_r G(\mathbf{r}_d, \mathbf{r}; \lambda) \cdot \nabla_r G(\mathbf{r}, \mathbf{r}_s; \lambda)$$
$$,\tag{1}$$

in the first-order Born approximation assuming that light diffuses inside the medium.[18] In Eq.(1),

$\mathbf{r}_s$ and $\mathbf{r}_d$ are the positions of the source and the detector on the boundary, respectively; $\delta\mu_a(\mathbf{r}; \lambda)$

$= \mu_a(\mathbf{r}, \lambda) - \mu_{a0}(\lambda)$ and $\delta D(\mathbf{r}; \lambda) = D(\mathbf{r}; \lambda) - D_0(\lambda)$ are the differences in absorption coefficient

and diffusion coefficient, respectively, between the target at $\mathbf{r}$ and the background, c is the speed

of light in the medium, and $G(\mathbf{r}, \mathbf{r}'; \lambda)$ is the Green's function describing light propagation from $\mathbf{r}'$

to $\mathbf{r}$ inside the background turbid medium of absorption and diffusion coefficients $\mu_{a0}(\lambda)$ and

$D_0(\lambda)$ where λ is the wavelength of the probing beam.

OPTICA treats each target within the scattering medium to be a virtual source and

expresses the change of the light intensity on the boundary of the specimen as:

$$-\Delta I(\mathbf{r}_d, \mathbf{r}_s; \lambda) = \sum_j a_j(\mathbf{r}_d; \lambda) s_j(\mathbf{r}_s; \lambda),\tag{2}$$

where $s_j(\mathbf{r}_s)$ represents the *j*-th target illuminated by the incident wave at $\mathbf{r}_s$, and $a_j(\mathbf{r}_d)$ is the

weighting matrix describing the propagation of light from the *j*-th target to the detector at $\mathbf{r}_d$. The

detected change of the light intensity -ΔI is hence a linear mixture of signals where a_j and s_j can

now be interpreted as the *j*-th weighting matrix and virtual source, respectively. Owing to the

statistical independence between these virtual sources, independent component analysis of -ΔI

measured at all scanning positions $\mathbf{r_s}$ and probing wavelengths λ yields a list of independent

components and recover both a_j and s_j. The number of the leading independent components (ICs)

gives the number of objects. The location of the *j*-th target is obtained from an analysis of the

retrieved IC (a_j and s_j) which relates directly to the source-to-object and object-to-detector

Green's functions $G(\mathbf{r}_j, \mathbf{r}_s; \lambda)$ and $G(\mathbf{r}_d, \mathbf{r}_j; \lambda)$ and the optical property of the target where $\mathbf{r}_j$ is the

position of the *j*-th target.[10-13] The explicit dependence on wavelength λ will be omitted hereafter

for brevity.

For the slab geometry investigated here, there are three virtual sources of specific patterns (one

centrosymmetric and two dumbbell-shaped) associated with each scattering target, and only one

centrosymmetric virtual source associated with each absorptive target. Among the three virtual

sources associated with a scattering target, the centrosymmetric virtual source is the strongest,

and more amenable to detection inside a *thick* highly scattering medium. The centrosymmetric

virtual source and the corresponding weighting matrix are $s_j \propto G(\mathbf{r}_j, \mathbf{r}_s)$ and $a_j \propto G(\mathbf{r}_d, \mathbf{r}_j)$, and

$s_j \propto dG(\mathbf{r}_j, \mathbf{r}_s)/dz$ and $a_j \propto dG(\mathbf{r}_d, \mathbf{r}_j)/dz$, respectively, for absorptive and scattering targets. A

simple least square fitting of the centrosymmetric component, such as

$$\min_{r_j, \alpha_j, \beta_j} \left\{ \sum_{\mathbf{r}_s} \left[\alpha_j^{-1} s_j(\mathbf{r}_s) - G(\mathbf{r}_j, \mathbf{r}_s) \right]^2 + \sum_{\mathbf{r}_d} \left[\beta_j^{-1} a_j(\mathbf{r}_d) - G(\mathbf{r}_d, \mathbf{r}_j) \right]^2 \right\}, \tag{3}$$

for the *j*-th absorptive object, can be used to yield the 3-*D* location r_j and the strength $\alpha_j \beta_j$ of the

target above (or, below) that of the surrounding medium in which the target is embedded. When

a priori knowledge about the property of the target is not available, Eq. (3) can still be used to

estimate the 3-D location of the target regardless absorption or scattering property of the target.

This follows from the fact that $dG(\mathbf{r}_j, \mathbf{r}_s)/dz \simeq -\kappa G(\mathbf{r}_j, \mathbf{r}_s)$, and $dG(\mathbf{r}_d, \mathbf{r}_j)/dz \simeq \kappa G(\mathbf{r}_d, \mathbf{r}_j)$, where

$\kappa = \sqrt{(\mu_{ao} - i\omega/c)/D_o}$ is chosen to have a nonnegative real part with ω the modulation frequency

of the incident wave. In this case, the strength of the target corresponds to

$$\alpha\beta = (\delta\mu_a + \frac{\kappa^2\delta\mu_s'}{3\mu_s'^2})Vc,$$ (4)

using Eq. (1) where V is the volume of the target and $\delta\mu_s' = \mu_s' - \mu_{s_0}'$ is the difference in the

reduced scattering coefficient between the target and the medium. Under illumination by

continuous wave light ($\omega=0$), the strength reduces to

$$\mu_s'^{-1}c(\mu_{a_0}\delta\mu_s' + \mu_{s_0}'\delta\mu_a)V = \mu_s'^{-1}c\delta(\mu_a\mu_s')V,$$

for an absorptive and/or scattering target. The quantity $\Lambda = \delta(\mu_a\mu_s')V$ pertains explicitly to the

target and has the dimension of length. We will refer to Λ as the "perturbation length of the

target" in subsequent discussion.

The signal of the j-th target is simply given by $-\Delta I_j = a_j(\mathbf{r}_d)s_j(\mathbf{r}_s)$. On the other hand, the

centrosymmetric signal from the j-th target can be approximated as a double convolution

$$-\Delta I(\mathbf{r}_d, \mathbf{r}_S) = \int G(\mathbf{\rho}_d - \mathbf{\rho}, z_d, z_j)X_j(\mathbf{\rho})G(\mathbf{\rho} - \mathbf{\rho}_s, z_j, z_S)d\mathbf{\rho},$$ (5)

where the integration is over the $z = z_j$ plane, X_j represents the target, $\mathbf{\rho}_d$ and $\mathbf{\rho}_s$ are the lateral

coordinates of the detector and the source, respectively. The cross section image of the j-th

target, X_j, is a 2-D map of the absorption/scattering strength of the target on the $z = z_j$, plane. In

the Fourier space, the target function can be obtained from Eq. (4) as,

$$X_j = -\frac{\Delta I_j(\mathbf{q} - \mathbf{q_s}, \mathbf{q_s})}{G(\mathbf{q} - \mathbf{q_s}, z_d, z_j)G^*(\mathbf{q_s}, z_j, z_s)} = -\frac{\Delta I_j(\mathbf{q}, 0)}{G(\mathbf{q}, z_d, z_j)G^*(0, z_j, z_s)},$$ (6)

where $\mathbf{q}$ and $\mathbf{q_s}$ are the spatial frequency on the lateral plane, and " $*$ " denotes complex

conjugate. We have chosen $\mathbf{q_s} = 0$ in the evaluation of the target function in Eq. (6) since sources

7

are usually much sparser than detectors in our setup where a charge coupled device (CCD) camera is used to detect the emergent light intensity distribution on the sample surface. The inverse Fourier transforms of $X_j(\mathbf{q})$ yields the high-resolution cross-section image of the *j*-th target due to the high density of detecting pixels of the CCD. The full-width at half-maximum (FWHM) spread of the cross section image X_j provides an estimate of the transverse size of the target.

3. Experimental Methods and Materials

The experimental arrangement for detecting and locating the tumors in the realistic model breast using OPTICA is shown schematically in Fig. 1. The model breast was assembled using two pieces of normal *ex vivo* female human breast tissues and two pieces of cancerous tissues provided by National Disease Research Interchange (NDRI) under an Internal Review Board approval at the City College of New York. The normal breast tissue specimens weighed 119 grams and 127 grams and consisted primarily of adipose tissue, while each tumor (infiltrating ductal carcinoma) pieces weighed approximately 1 gram. Two incisions were made in the mid-plane (along the z-axis, which was the shortest dimension) of normal tissue pieces and a small amount of tissue was removed from the core region to make two small pouches. The tumor pieces were inserted into these pouches, and the incisions were closed by moderate compression of the tissue-tumor composite from all directions. The sample was placed inside a cylindrical transparent plastic container with a movable end face of diameter 110 mm, which was moved to slightly compress the tissue along the *z*-axis and hold it in place. The resulting slab sample filled over 75% of the lateral dimension of the cylinder and had a uniform thickness of 40 mm. It was treated as a single entity in the subsequent imaging experiments. The nominal dimension of the tumor piece located at the left side of the sample ('left tumor') was 8 mm x 5 mm x 3 mm and

that located on the right side ('right tumor') was 10 mm x 10 mm x 5 mm. The positions of the tumor pieces within the sample, and the distance between the pieces were known approximately, as those were placed in position as discussed above. The axial orientation of the plastic container and sample within it was preserved for magnetic resonance imaging (MRI) experiments following the optical measurements.

The optical imaging experiments were carried out using the 750 nm, 800 nm, and 830 nm near-infrared beams from a continuous wave Ti:sapphire laser. The average beam power was maintained at 10 mW for every wavelength. The light beam at any of these wavelengths was collimated to a 1-mm spot onto the entrance face (henceforth referred to as the 'source plane') of the slab sample. Multiple source illumination was realized in practice by step scanning the slab sample along the horizontal (x) and vertical (y) directions across the laser beam in an x-y array of grid points using a computer controlled translation stage. A camera lens collected the diffusely transmitted light on the opposite face of the sample (henceforth referred to as the 'detection plane') and projected it onto the sensing element of a cooled 16 bit, 1024 X 1024 charged couple device (CCD) camera. Each illuminated pixel of the 1024 x 1024 pixels of the CCD camera could be regarded as a detector. For illumination of every scanned point on the source plane, the CCD camera recorded the diffusely transmitted intensity pattern on the detection plane. A 62.5 mm X 37.5 mm area of the source plane was scanned in a 26 X 16 array of x-y grid points with a step size of 2.5 mm, while the CCD camera imaged the entire detection plane.

For MRI experiments, the breast model sample in the plastic container was taken to Memorial Sloan-Kettering Cancer Center (MSKCC) small animal MRI facility. The facility currently utilizes a 4.7-T 33-cm bore magnet imaging/spectroscopy system (Bruker BioSpin) operating at 200 MHz for 1-H (standard) imaging experiments for imaging of rats and mice. The

tissue container was fixed inside the radio-frequency coil (RFC) and placed inside the bore magnet. MR images of the sample were recorded in 2.0-mm slice thick sagittal slices.

4. Results

The average of all 26 X 16 images was used to assess the average optical properties of the *ex vivo* model breast. The radial profile of the transmitted light intensity of the average image was fitted to the predictions of a diffusion model of light propagation inside a slab. Assuming a typical value of 1 mm^{-1} for the reduced scattering coefficient for breast tissues, the average absorption coefficient, μ_a of the entire model breast was found to be 0.00338 mm^{-1}, 0.00238 mm^{-1} and 0.00350 mm^{-1} for wavelengths of 750, 800 and 830 nm, respectively. While the entire detection plane was imaged, each raw image was cropped to retain the region within 76 mm X 66 mm for carrying out image reconstruction. The size of 1 pixel in the raw image was 165 μm X 165 μm. The raw images were binned by merging 5 x 5 pixels into one to enhance the signal-to-noise ratio. All the binned images corresponding to probing of the grid points in sequence were then stacked, and used as input for independent component analysis.

Figures 2(a) display the OPTICA generated independent light intensity distributions on the detector plane for left tumor (left pane) and the right tumor (right pane) for the probe wavelength of 750 nm. Corresponding bottom panes in Fig. 2(b) show the Green's function fit (solid line) to horizontal (circles) and vertical (triangle) spatial profiles through the center of intensity distributions along the dashed line. Similar results are obtained for probing wavelengths of 800 nm and 830 nm, as well. Table I presents the (*x, y, z*) locations of the two tumor pieces derived from the least square fitting process using Eq. (3) for measurements at all three wavelengths. While the tumor pieces have finite spatial dimension as noted in sample description, the location gives the coordinates of a point which is taken to be the peak of the spatial intensity distribution,

and will be referred to as the 'center' of the tumor piece in subsequent discussion. The three estimates of tumor locations from measurements using the three wavelengths agree well with one another. The center of right tumor is estimated to be at a distance of 21.6 mm from the detection plane and to be located at (54.8, 50.1, 18.4) mm. The coordinates quoted above are averages of the three estimates from measurements at the three wavelengths. Similarly, the center of the left tumor is estimated to be 19.6 mm away from the detection plane, and located at (48.4, 26.8, 20.4) mm.

The cross-section images of the left tumor and the right tumor obtained using the 2-D inverse Fourier transform formalism pertaining to Eq. (5) appear in the left pane and right pane of Fig. 3(a), respectively. The corresponding bottom panes of Fig. 3(b) display the spatial intensity profiles of the cross-section image along the *x*- and *y*-directions. The full width at half maximum (FWHM) values of these intensity profiles is taken to estimate of the lateral dimensions of the left tumor to be 12.6 mm X 8.2 mm and that of the right tumor to be 9.9 mm X 9 mm. These estimates are comparable to the known lateral dimensions of the tumors.

Table I also lists, for the three wavelengths, the perturbation length, Λ of the two tumors. The strength decreases as wavelength increases for the two tumors and the three wavelengths of light used in the measurements.

5. Discussion

The results presented above demonstrate that OPTICA could detect and locate the two tumor pieces inside the model breast with considerable accuracy. Comparison of Fig.2 and Fig.3 reveal that the cross-section images obtained using back-projection Fourier transform formalism are more compact than the OPTICA-generated spatial intensity distribution of independent components.

The MRI images of the sample displayed in Fig. 4 were obtained to serve as reference for testing the validity of the OPTICA measurements. The MRI measurements corroborate the OPTICA assessments in terms of the number of targets, the distance separating them, and their depth (z-position). OPTICA estimates a separation of ~ 2 mm between the centers of the two tumor pieces, while MRI places them in two sagittal slices that are 4 mm apart. Given that the MRI images were recorded for 2-mm thick slices, this is a good agreement between the results from the two methods. Similarly, both the approaches provide comparable estimates for overall distance between the tumor pieces.

Both ICA and back-projection overestimate the lateral dimensions of a target, which is a consequence of the highly diffuse nature of the light propagation in breast tissue. The estimated size of the right tumor is consistent with this expected behavior and its position coordinates agreed well with the known position within the sample. However, the left tumor appeared much extended along the x-direction in the ICA analysis, and exhibited two lobes in the cross-section image. ICA took the location to be in the middle and returned an estimate of x coordinate that was not in good agreement with the known location of the left tumor, and did not follow the level of accuracy that we have obtained in locating targets embedded in model media and *ex vivo* breast tissue specimens.[12, 13] The left lobe of the cross-section image is more intense than the right lobe. The location of the center of the left lobe is consistent with the known location of the left tumor, and corresponds to the more intense part of the MR image of the left tumor. The distance between this left lobe of the cross-section image of left tumor and center of the right tumor is estimated to be ~35 mm, which is in excellent agreement with the MRI result. However, the estimated cross section of the left lobe alone is significantly higher than the known size of the left tumor, even when a higher estimate due to diffusive nature of light propagation is taken into

consideration. The MR images also exhibit a region around the left tumor that has higher contrast than the most of the surrounding normal tissue, but a lower contrast than the image of the left tumor. It seems that the left tumor was embedded within a substructure that had different characteristics than the surrounding normal tissue. The nature of the substructure could not be assessed from our OPTICA or MRI measurements. A pathological analysis could have provided additional information.

While the three wavelengths that we used were not targeted for obtaining diagnostic molecular spectroscopic information, we observed some instructive and clarifying advantages of employing light of different wavelengths. In addition to the two tumor pieces and the lower-contrast substructure around left tumor shown in Fig. 2 and Fig. 3, another independent component (not shown in any figure) appeared prominently in OPTICA analysis of experiments conducted using all three wavelengths. However, strength of two of the independent components corresponding to tumor pieces decreased monotonically with increasing wavelength of the probing light, but no such wavelength dependence was observed in the strength of the third independent component. We tentatively ascribe this feature to an embedded water pocket within the sample. Multi-wavelength measurements helped sort out this artifact. The monotonic decrease in strength of the tumor pieces with increasing wavelength is consistent with the wavelength dependence of light scattering by tissue and tumor constituents.

The scattering strength αβ of the target can obtained from fitting to the OPTICA images, from which the 'perturbation length' $\Lambda = \delta(\mu_a\mu_s')V$, of the target can be computed. The values of Λ for the left tumor are 13.9 mm, 9.5 mm, and 8.9 mm at the wavelength 750 nm, 800 nm, and 830 nm, respectively. The Λ–values of the right tumor are 20.3mm, 14.0mm, and 11.9 mm at these three wavelengths, respectively. The monotonic decrease in strength of the tumor pieces

with increasing wavelength is consistent with the wavelength dependence of light scattering by

tissue and tumor constituents. It further indicates that scattering is the dominant contrast

mechanism for these wavelengths.

The perturbation length and strength of the right tumor are found to be higher than those of the

left tumor. Real difference could be substantially higher, since OPTICA overestimated the size

of the left tumor.

Acknowledgements

REFERENCES

1. A.P. Gibson, J.C. Hebden, and S.R. Arridge, "Recent advances in diffuse optical imaging," *Phys Med Biol.* **50** R1-43 (2005).

2. S. Nioka, M. Miwa, S. Orel, M. Shnall, M. Haida, S. Zhao, and B. Chance, "Optical imaging of human breast cancer," *Adv Exp Med Biol.* **361**, 171-9 (1994).

3. H. Dehghani, B. W. Pogue, S. P. Poplack, and K. D. Paulsen, "Multiwavelength three-dimensional near-infrared tomography of the breast: initial simulation, phantom, and clinical results," *Appl. Opt.* **42**, 135, (2003).

4. H. Rinneberg, D. Grosenick, K.T. Moesta, J. Mucke, B. Gebauer, C. Stroszczynski, H. Wabnitz, M. Moeller, B. Wassermann, and P.M. Schlag, "Scanning time-domain optical mammography: detection and characterization of breast tumors *in vivo*," *Technol. Cancer Res. Treat.* **4**, 483-96 (2005).

5. A. Corlu, R. Choe, T. Durduran, K. Lee, M. Schweiger, S.R. Arridge, E.M. Hillman, and A.G. Yodh, "Diffuse optical tomography with spectral constraints and wavelength optimization," *Appl. Opt*. **44**, 2082-93 (2005).

6. A. Li, E.L. Miller, M.E. Kilmer, T.J. Brukilacchio, T. Chaves, J. Stott, Q. Zhang, T. Wu, M. Chorlton, R.H. Moore, D.B. Kopans, and D.A. Boas, "Tomographic optical breast imaging guided by three-dimensional mammography," *Appl. Opt.* **42**, 5181-90 (2003).

7. A.E. Cerussi, D. Jakubowski, N. Shah, F. Bevilacqua, R. Lanning, A.J. Berger, D. Hsiang, J. Butler, R.F. Holcombe, and B.J. Tromberg, "Spectroscopy enhances the information content of optical mammography," *J Biomed Opt*. **7**, 60-71 (2002).

8. A. H. Gandjbakhche, V. Chernomordik, J. C. Hebden, and R. Nossal, "Time-dependent contrast functions for quantitative imaging in time-resolved transillumination experiments," *Appl. Opt.* **37**,1973 (1998).

9. W. Cai, S. K. Gayen, M. Xu, M. Zevallos, M. Alrubaiee, M. Lax, and R. R. Alfano, "Optical three-dimensional inverse image reconstruction of objects in turbid media from ultrafast time-sliced optical transmission measurements," *Appl. Opt.* **38**, 4237 (1999).

10. M. Xu, M. Alrubaiee, S. K. Gayen and R. R. Alfano, "Optical imaging of turbid media using independent component analysis: theory and simulation," *J. Biomed. Opt.* **10**, 051705-1-051705-12 (2005).

11. M. Xu, M. Alrubaiee, S. K. Gayen and R. R. Alfano, "Three-dimensional localization and optical imaging of objects in turbid media using independent component analysis," *Appl. Opt.* **44**, 1889-1897 (2005).

12. M. Alrubaiee, M. Xu, S. K. Gayen, M. Brito, and R. R. Alfano, "Three-dimensional optical tomographic imaging of objects in tissue-simulating turbid medium using independent component analysis," *Appl. Phys. Lett.* **87**, 191112 (2005).

13. M. Alrubaiee, M. Xu, S. K. Gayen, and R. R. Alfano, "Three-dimensional localization and cross section reconstruction of fluorescent targets in *ex vivo* breast tissue using independent component analysis," *Appl. Phys. Lett.* **89**, 133902 (2006).

14. P. Comon, "Independent component analysis – A new concept," *Signal-Processing* **36**, 287 (1994).

15. A. J. Bell, "Information theory, independent component analysis, and applications," in *Unsupervised Adaptive Filtering,* vol. I, S. Haykin, ed., New York, Wiley, (2000), pp. 237–264.

16. M. A. O'Leary, D. A. Boas, B. Chance, and A. G. Yodh, "Experimental images of heterogeneous turbid media by frequency-domain diffusing-photon tomography," *Opt. Lett.* **20**, 426–428 (1995).

17. M. Xu, M. Lax, and R. R. Alfano, "Time-resolved Fourier optical diffuse tomography," *J. Opt. Soc. Am. A* **18**, 1535–1542 (2001).

18. P. M. Morse and H. Feshbach, *Methods of Theoretical Physics*, vol. I and II, New York: McGraw-Hill, 1953.
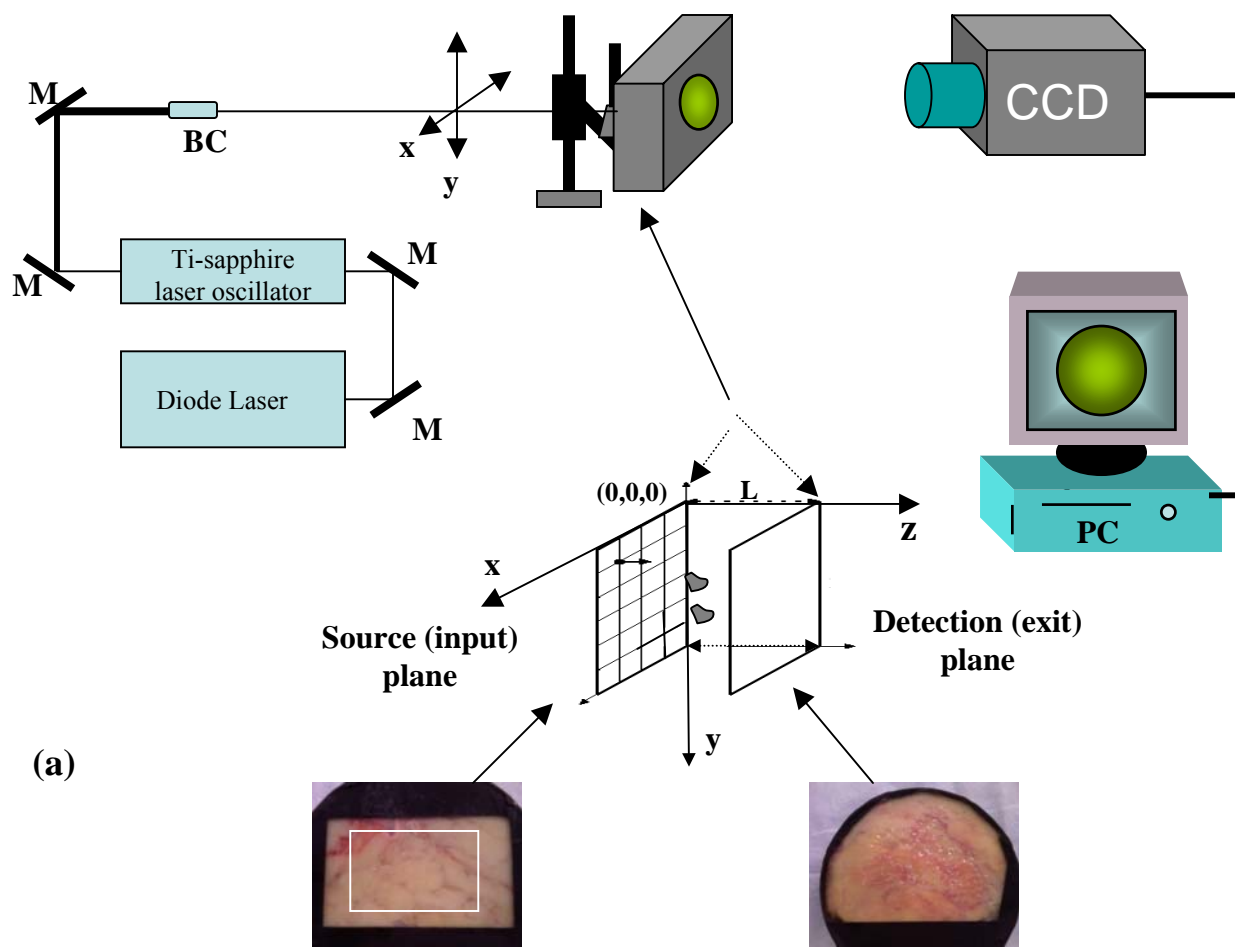
Figure Captions

1. (a) Schematic diagram of the experimental arrangement. (Key: BC = beam collimator, CCD = charge coupled device, M = mirror.) Inset below shows the expanded view of the source (input) plane with the scanning grid points. (b) Photographs of the source plane (left) showing the scanned area, and detection plane (right) of the model breast sample. (c) (Upper pane) Typical raw CCD image of the detection plane, and how it is cropped and binned for analysis. (Lower pane) Flow chart of steps in the analysis process.

2. (a) OPTICA generated independent intensity distributions on the detection plane ($z = 40$ *mm*) for the left tumor piece (left pane) and the right tumor piece (right pane) for measurements carried out using 750-nm light. (b) Corresponding bottom panes show the Green's function fits (solid lines) to the spatial intensity profiles along the *x*-axis (denoted by circles) and *y*-axis (denoted by triangles) denoted by the white lines.

3. (a) Cross section images of the left tumor piece (left pane) and the right tumor piece (right pane) formed by back projection onto the transversal plane at their respective *z*-positions. (b) Bottom panes show the corresponding spatial intensity profiles along the *x*- and *y*-axes denoted by the white lines.

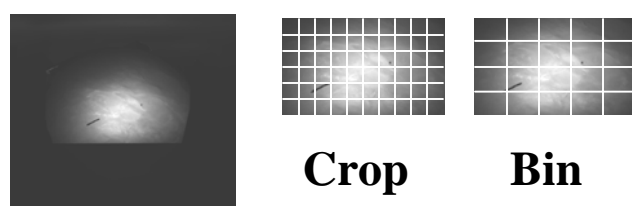4. Magnetic resonance images of the left tumor and the right tumor pieces.

Table I Coordinates (x, y, z) and perturbation length, Λ of the tumors

Wavelength (nm)	Left Tumor		Right Tumor	
	Position (x, y, z) (mm)	Λ (mm)	Position (x, y, z) (mm)	Λ (mm)
750	(26.4, 48.6, 20.2)	13.9	(50.3, 54.4, 20.0)	20.3
800	(27.2, 49.4, 19.5)	9.5	(49.4, 54.4, 17.9)	14.0
830	(27.2, 47.8, 21.5)	8.9	(50.4, 55.2, 17.2)	11.9
	(26.9, 48.6, 20.4)*		**(50.0, 54.7, 18.4)***	

* Bottom row gives the averages of the positions obtained from three wavelengths

(a)

(b)

(c)

Crop   Bin

| ICA | Obtain Leading ICs | Fit $G(r,r_s)$, $G(r,r_d)$ to ICs | Planar image of each IC |

Fig. 1

(a)

(b)

Fig. 2

(a)

(b)
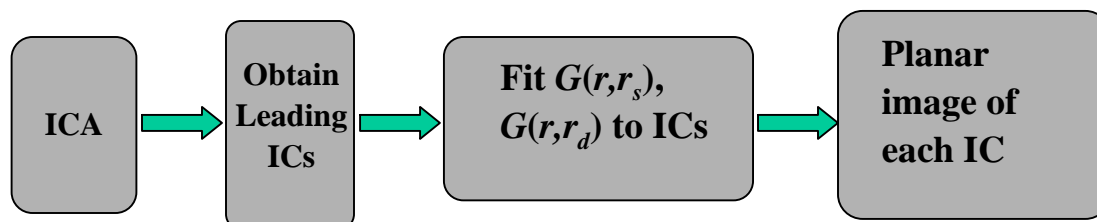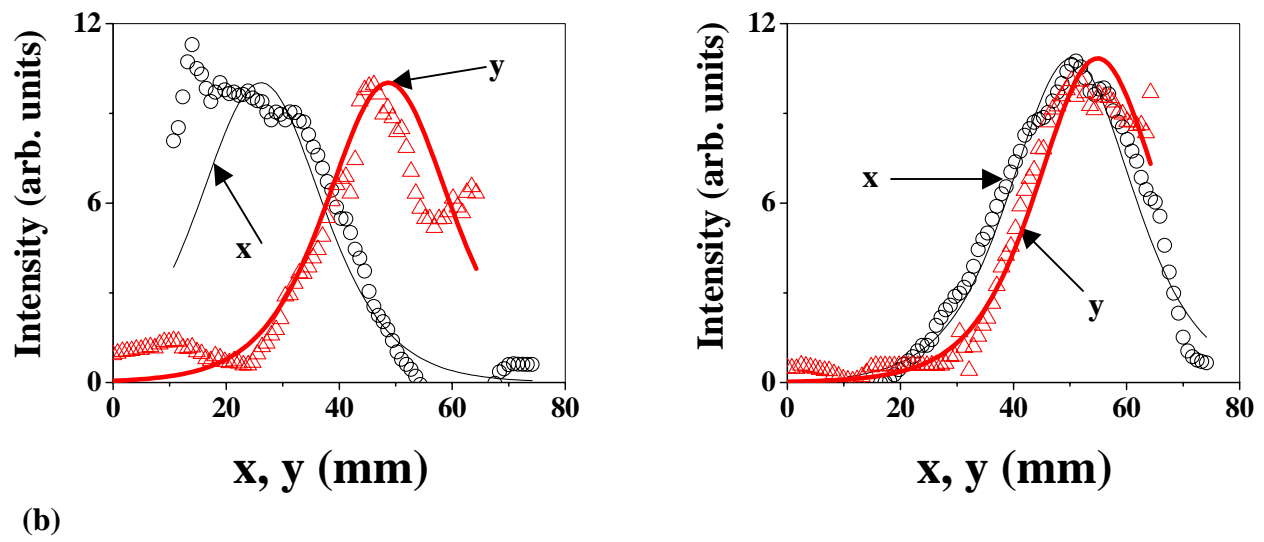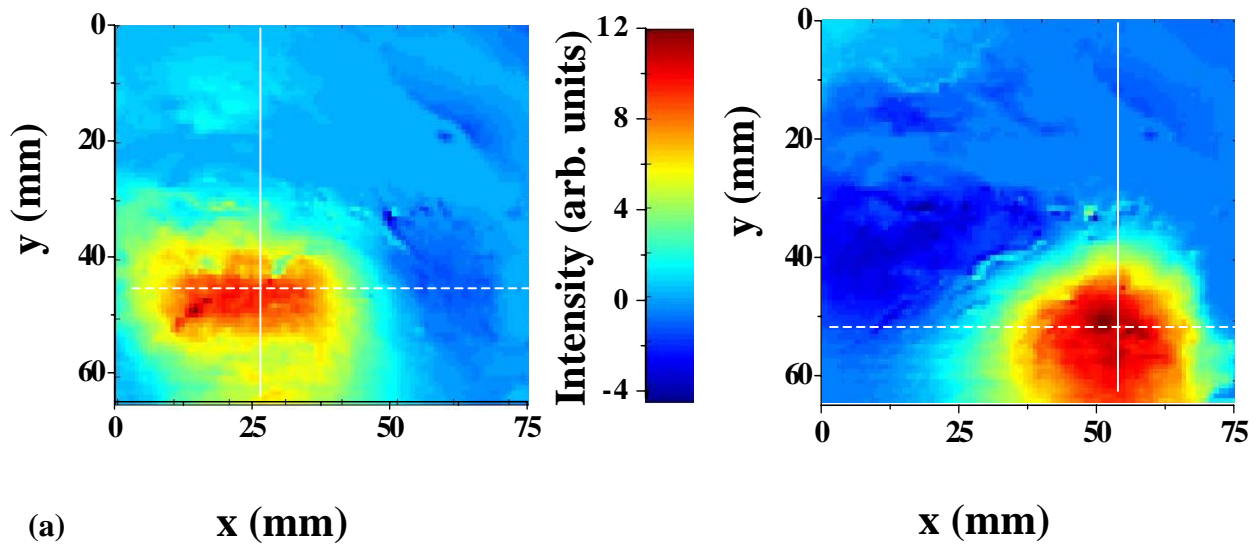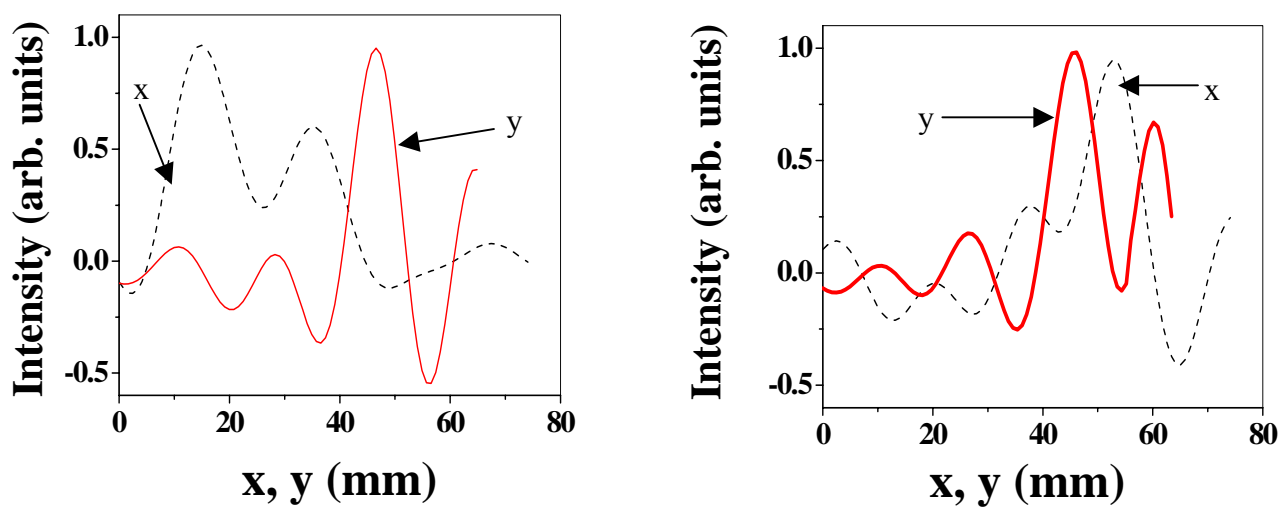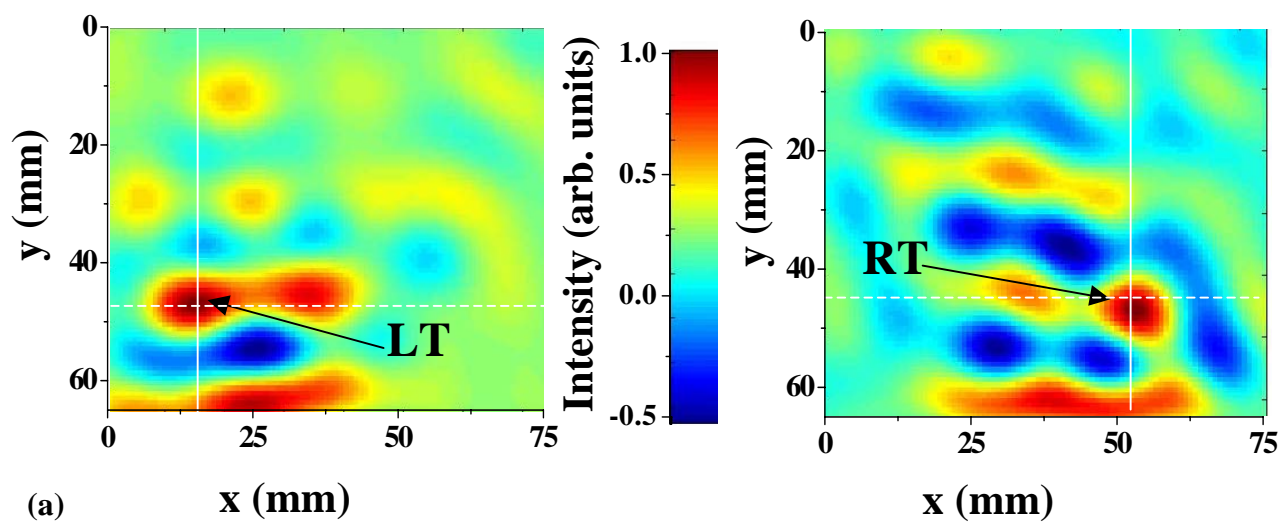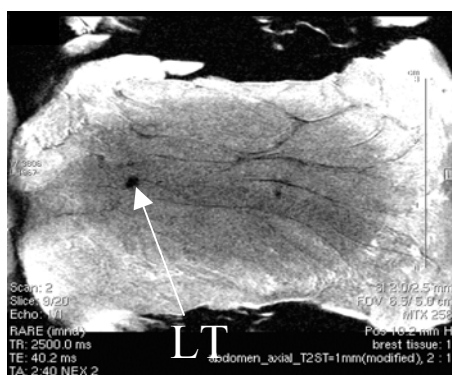
Fig. 3

(a) (b)

Fig. 4

Optical Imaging of Objects in Turbid Media using Principal Component Analysis and Time Reversal Matrix Methods

Binlin Wu[1], M. Alrubaiee[1], W. Cai[1], M. Xu[2] and S. K. Gayen[1]

[1]*The Institute for Ultrafast Spectroscopy and Lasers, Physics Department*
The City College and the Graduate Centre of The City University of New York, New York, NY 10031, USA
[2]*Physics Department, Fairfield University, Fairfield, CT 06824, USA*
Email: bwu@sci.ccny.cuny.edu

Abstract: Principal Component Analy sis and Time Rev ersal Matrix methods were used to develop approaches for i maging of targ ets in turbid m edia. Th e efficacy is d emonstrated b y imaging t wo targ ets embedded in Intralipid-10% suspension in water.
@2009 Optical Society of America
OCIS codes: (110.0113) Imaging through turbid media; (170.3880) Medical and biological imaging

1. Introduction

Fast and accurate methods are needed for detection and localization of targets embedded in turbid media. In this paper, we present two algorithms based on Principal Component Analysis (PCA) [1] and Multiple Signal Classification (MUSIC) to the eigenvectors of a Time Reversal (TR) matrix [2-3] for obtaining images and location information of targets in turbid media. We refer to these approaches as Optical Imaging using Principal Component Analysis (OIPCA) and Time Reversal Optical Tomography (TROT).

2. Formalism and Experimental Arrangement

A multi-source probing and multi-detector signal acquisition scheme to obtain multiple angular views of the target(s) was used for both methods. When using OIPCA, the leading eigenvalues provided the number and strengths of targets. Light propagation from different targets to the source plane and detector plane was considered to be uncorrelated and decomposed from the recorded data. The location of the objects was retrieved by fitting the principal components of intensity distributions (PCID) to Green's functions. When using TROT, a Time Reversal (TR) matrix was constructed by multiplying the response matrix by its adjoint matrix (transpose for continuous-wave (CW) illumination). The signal and noise subspaces were calculcated and separated using a method similar to L-curve regularization. The eigenvectors with leading non-zero eigenvalues of the TR matrix correspond to the embedded objects, which are orthogonal to the vectors in the noise subspace. The vector subspace method, MUSIC, along with Green's functions calculated from an appropriate forward model, was then used to determine the locations of the embedded objects.
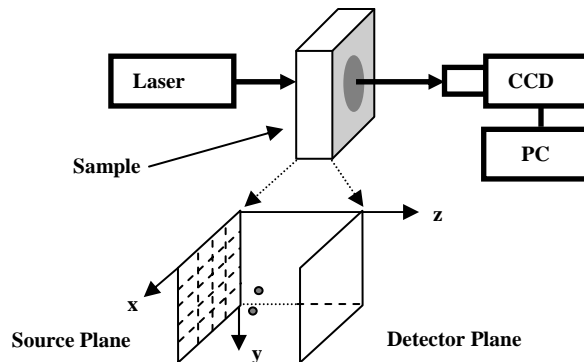

Fig. 1. A schematic diagram of the experimental arrangement used for imaging objects embedded in a turbid medium. Inset shows the 2D array in the input plane that was scanned across the incident laser beam.

The sample shown schematically in Fig. 1, was a 250 mm × 250 mm × 50 mm transparent plastic container filled with Intralipid-10% suspension in water, and two absorptive targets were embedded in it. The concentration of Intralipid-10% was adjusted to provide a transport mean free path $l_t \sim 1.43$ mm and an absorption coefficient $\mu_a = 0.003$ mm^{-1} at 785 nm. The targets, two ~ 10-mm diameter glass spheres filled with indocyanine green dye solution in water ($\mu_a = 1.15$ mm^{-1}), were placed at 20 mm and 25 mm away from the entrance face, respectively. The sample was scanned at 11×12 grid points with a step size of 5 mm. The transmitted signal at 785 nm from the exit plane was recorded by a CCD camera. From each image, a 53.4 mm ×53.4 mm window was cropped out and then 5×5 pixels of each image were binned to one. Then OIPCA and TROT analysis were performed separately.

3. Results

The OIPCA generated PCIDs of target 1 on the detector plane and source plane are shown in Figs. 2(a,c). Fitting of PCIDs to Green's functions are shown in Fig. 2(b,d). Similar images were obtained for target 2.
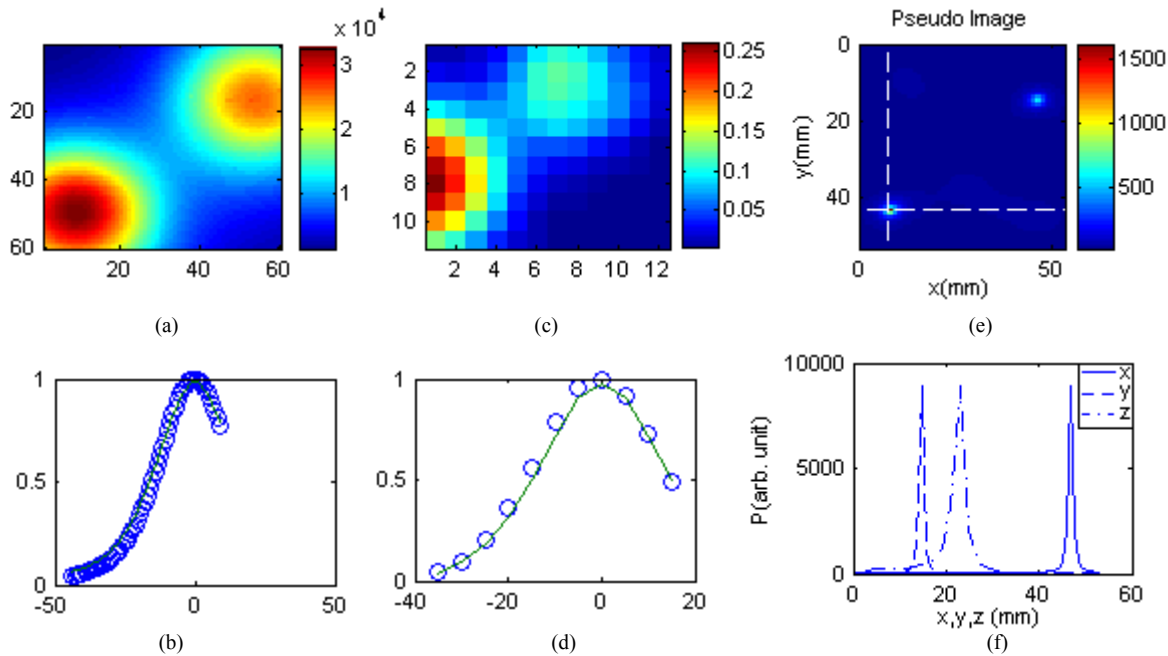

(a)

(c)

(e)

(b)

(d)

(f)

Fig 2. For target 1, OIPCA generated intensity distributions on the detector and source planes are shown in (a) and (c), respectively; Green's functions fit to the vertical spatial profiles through the maxima are shown in (b) and (d), respectively. TROT generated cross-section pseudo image is shown in (e) and pseudo value profiles through the target along x, y and z directions are shown in (f).

TROT found the absorptive objects and generated pseudo images using pseudo spectrum from MUSIC. The pseudo image and its profile for target 1 are shown in Fig. 2(e,f). Similar images for target 2 were obtained. Locations of the objects found by OIPCA and TROT are listed and compared with known locations in Table I.

Table I: Target positions determined by OIPCA and TROT

Objects	Known Positions (x, y, z) (mm)	OIPCA retrieved positions (x, y, z) (mm)	TROT retrieved positions (x, y, z) (mm)
1	(46.5, 14.5, 20)	(46.7, 14.7, 19.5)	(46.7, 14.7, 21)
2	(9.2, 44.5, 25)	(7.6, 44, 24.8)	(7.6, 43.2, 25)

4. Summary

Both methods detected the targets and provided their locations that are in good agreement with known positions. Experiments involving tumors in model breast assembled using *ex vivo* breast tissues are in progress.

5. References

[1] M. Stetter, I. Schießl, T. Otto, F. Sengpiel, M. Hübener, T. Bonhoeffer and K. Obermayer, "Principal component analysis and blind separation of sources for optical imaging of intrinsic signals," *NeuroImage*, **11**, 482-490 (2000).
[2] A. J. Devaney, "Time reversal imaging of obscured targets from multistatic data," *IEEE. Trans Ant & Prop.* **53,** 1600-1610 (2005).
[3] W. Cai, M. Alrubaiee, S. K. Gayen, M. Xu, R. R. Alfano, "Three-dimensional optical tomography of objects in turbid media using the round-trip matrix, " *Proc. SPIE* **5693**, 4 (2005).

Appendix 4: A copy of the Technical Abstract of a research proposal entitled,
"Nanocomposite-Chemokine Mimic Conjugates for Imaging and Prevention of Breast Cancer Metastases"
submitted to the 2010 Breast Cancer Research Program of CDMRP

Attachment 3: Technical Abstract

Background: Breast cancer metastases are responsible for the 90% mortality and morbidity in breast cancer. The current therapies, surgery, radiation, chemotherapy, and a combination of these, do not prevent formation of metastases. The current imaging techniques have major limitations, the less than optimal sensitivity to detect micrommetastases, and the inability to detect specific cancer cell-surface markers. Clearly there is a need to develop new imaging probes that are highly sensitive and biospecific to help diagnosis, and there is an acute need to develop therapies that prevent metastasis.

Objective/Hypothesis: The *hypothesis* to be tested in this research project is that synthetic chemokine mimics could interfere with the binding of natural chemokines (e.g., CXCL-12) to their receptor (e.g., CXCR4) located at the surface of tumor cells thereby preventing migration of tumor cells to metastatic sites. The *objective* of the proposed work is to develop self-targeting nanocomposites with an imaging module and a chemokine mimic-based therapeutic module integrated into a single entity for sensitive detection/ diagnosis, and to prevent formation of metastases by stopping migration of tumor cells to the target organs.

Specific Aims: The specific aims of the proposed research are: (1) Synthesis of imaging module, which is NIR emitting, biocompatible PbS, InAs, CdHgTe QD nanoparticles in dendrimer nanoreactors; (2) Synthesis of therapeutic module that includes: (a) Synthesis of the small molecule, non-peptidic chemokine mimics; (b) Synthesis of the conjugates of chemokine mimic and QD-dendrimer nanocomposite; (c) Structural optimization of the chemkine mimic-QD conjugates; (3) Study of spectroscopic properties of the QD-dendrimer nanocomposites, and conjugates of chemokine mimic and QD-dendrimer nanocomposite, and investigation of their efficacy as contrast agents in simulated breast imaging applications; (d) Study of the efficacy of the chemokine mimics and the conjugates in preventing cancer cell migration in a collaborative bioassay and animal study.

Study Design: To achieve a new paradigm in breast cancer treatment, self-targeting nanocomposites, with an imaging module and a therapeutic module integrated into a single entity will be synthesized. The imaging module will be loaded with NIR nanoparticle fluorescers to enable highly sensitive detection and diagnosis. The therapeutic module will be loaded with multiple copies of chemokine mimic homing devices, and will be deployed to prevent organ-specific tumor cell migration that leads to metastases. It is the chemokine mimics in the therapeutic module that that will self-target the combined modules to the CXCR4 expressing tumor cells, and it is the nanoparticles in the imaging module that will enable to detect and visualize the tumor cells. Spectroscopy and optical imaging studies of the imaging module, the therapeutic module and the combination of them, as well as bioassay-directed structural optimization of the chemokines and their conjugates will be integrated with the syntheses, and will be conducted throughout the course of the whole project.

Innovation: The project is highly innovative in many ways: (a) It introduces the paradigm of early detection and prevention through synthesis of conjugates with a imaging module and a therapeutic module in the same nanostructure; (b) The synthesis process brings together the concept of multivalency, the idea of chemokine mimics as agents for prevention of cancer cell migration, and use of dendrimers as stabilizer and nanoreactor for fluorescent entity synthesis, all of which are novel ideas in other areas and are being proposed to tackle the problem of breast cancer; (c) the prospect of using NIR light based noninvasive approach for early detection and potential diagnosis based on molecular spectroscopic signatures is proposed to be further enhanced through design of efficient fluorescent agent.

Impact: The proposed project is expected to have profound impact on the early detection of breast cancer, when it is more amenable to treatment; as well as, on the prevention of metastases that lead to mortality and morbidity.